Characterization of a micromachined membrane deformable mirror

ULRIKA LARSSON

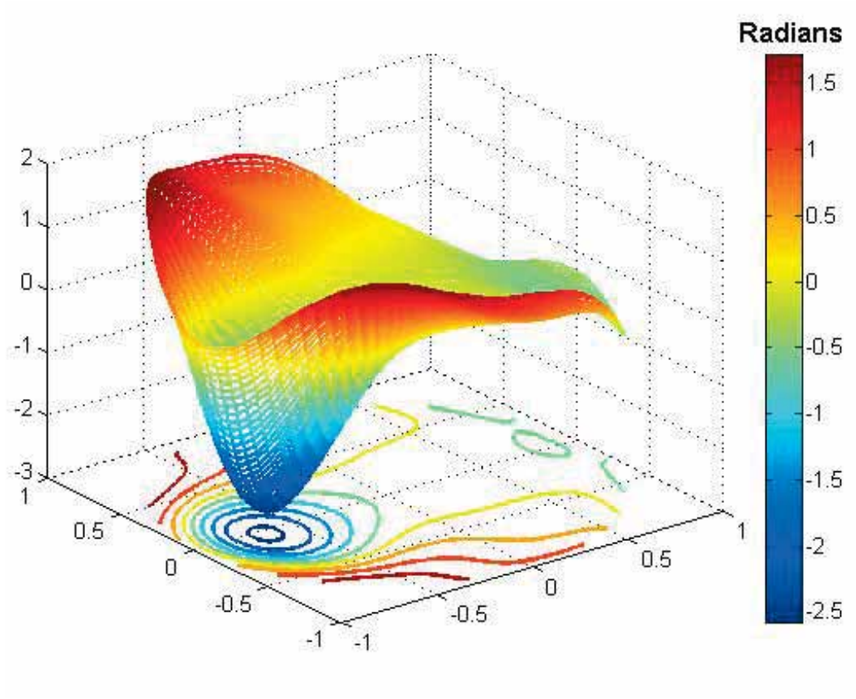

FOI is an assignment-based authority under the Ministry of Defence. The core activities are research, method and technology development, as well as studies for the use of defence and security. The organization employs around 1350 people of whom around 950 are researchers. This makes FOI the largest research institute in Sweden. FOI provides its customers with leading expertise in a large number of fields such as security-policy studies and analyses in defence and security, assessment of different types of threats, systems for control and management of crises, protection against and management of hazardous substances, IT-security an the potential of new sensors.

FOI
Defence Research Agency
Sensor Technology
P.O. Box 1165
SE-581 11 Linköping

Phone: +46 13 37 80 00
Fax: +46 13 37 81 00

www.foi.se

FOI-R-- 1917 --SE Technical report
ISSN 1650-1942 May 2006

Sensor Technology

Ulrika Larsson

Characterization of a micromachined membrane deformable mirror

FOI-R--1917--SE
ISSN 1650-1942

Technical report
May 2006

Sensor Technology

Issuing organization	Report number, ISRN	Report type
FOI – Swedish Defence Research Agency Sensor Technology P.O. Box 1165 SE-581 11 Linköping	FOI-R--1917--SE	Technical report
	Research area code 6. Electronic Warfare and deceptive measures	
	Month year May 2006	**Project no.** E3020
	Sub area code 61 Electronic Warfare including Electromagnetic Weapons and Protection	
	Sub area code 2	

Author/s (editor/s)	
Ulrika Larsson	**Project manager** Lars Sjöqvist
	Approved by Ove Steinvall
	Sponsoring agency HKV
	Scientifically and technically responsible Lars Sjöqvist

Report title

Characterization of a micromachined membrane deformable mirror

Abstract

The purpose of this work was to evaluate a 37 channel micromachined membrane deformable mirror which is a component used in adaptive optics. Several transfer functions with different mirror bias shapes were determined and analyzed. An interferometer was used to measure and to evaluate the transfer functions. The capacity of the mirror to produce wavefronts containing single Zernike coefficients was tested with an open loop scheme. A closed loop scheme was used for one of the transfer functions to construct three different Zernike polynomials.

The results show that the mirror has a capacity to produce wavefronts using Zernike polynomials with coefficient values that have the magnitude of a few radians measured relative the bias. The number of the mirror eigenmodes used in the wavefront reconstruction was found to be of major importance. The closed loop reconstruction scheme enhanced the results in comparison to the open loop scheme.

Keywords

Adaptive optics, membrane deformable mirror, interferometer, wavefront reconstruction

Further bibliographic information	**Language** English
ISSN 1650-1942	**Pages** 36 p.
	Price acc. to pricelist

Utgivare	Rapportnummer, ISRN	Klassificering
FOI - Totalförsvarets forskningsinstitut Sensorteknik Box 1165 581 11 Linköping	FOI-R--1917--SE	Teknisk rapport
	Forskningsområde 6. Telekrig och vilseledning	
	Månad, år Maj 2006	**Projektnummer** E3020
	Delområde 61 Telekrigföring med EM-vapen och skydd	
	Delområde 2	

Författare/redaktör	Projektledare
Ulrika Larsson	Lars Sjöqvist
	Godkänd av Ove Steinvall
	Uppdragsgivare/kundbeteckning HKV
	Tekniskt och/eller vetenskapligt ansvarig Lars Sjöqvist

Rapportens titel

Karakterisering av en deformerbar membranspegel

Sammanfattning

Syftet med det är arbetet var att utvärdera en membranspegel med 37 kanaler som är en komponent som används inom adaptiv optik. Flera överföringsfunktioner med olika spänningsbias bestämdes och analyserades. En interferometer användes för att bestämma och utvärdera överföringsfunktionerna. Prestanda hos spegeln att representera vågfronter innehållande olika Zernikekoefficienter testades med ett öppen loop schema. En metod baserad på sluten loop användes för en överföringsfunktion för att rekonstruera tre olika Zernikepolynom.

Resultaten visar att spegeln kan representera vågfronter bestående av Zernikepolynom med koefficienter av storleksordningen några radianer relativt använd bias. Antalet egenmoder hos spegeln som används vid vågfrontsrekonstruktionen har stor betydelse. Ett rekonstruktionsschema baserat på sluten loop förbättrade resultaten i jämförelse med öppen loop.

Nyckelord

Adaptiv optik, membranspegel, interferometer, vågfrontsrekonstruktion

Övriga bibliografiska uppgifter	Språk Engelska
ISSN 1650-1942	**Antal sidor:** 36 s.
Distribution enligt missiv	**Pris: Enligt prislista**

CONTENT

1 INTRODUCTION 5

2 THEORY 5

2.1 OPTICAL WAVES 5
2.2 ADAPTIVE OPTICS 6
2.2.1 The deformable mirror 6
2.3 INTERFEROMETRY 7
2.3.1 The principle of a Michelson interferometer 7
2.3.2 Interferogram 8
2.3.3 Fourier transform analysis of interferogram 8
2.3.4 Quick Fringe 10
2.4 ZERNIKE POLYNOMIALS 10
2.5 DESCRIPTION OF THE MIRROR SURFACE 11
2.6 RECONSTRUCTION OF THE WAVEFRONT 13
2.7 WAVEFRONT ERROR 13

3 EXPERIMENTAL METHODS 14

3.1 EXPERIMENTAL SETUP 14
3.1.1 The interferometer 15
3.1.2 The control system 16
3.1.3 Technical details – the deformable mirror 16
3.2 DETERMINING THE TRANSFER FUNCTION 17
3.3 MIRROR CONTROL 18
3.4 ZERNIKE POLYNOMIAL PRODUCTION 19

4 RESULTS 19

4.1 VALIDITY OF THE FOURIER TRANSFORM METHOD 19
4.2 LINEARITY OF THE MIRROR 20
4.3 THE EIGENMODES OF THE MIRROR 21
4.4 DETERMINING THE BIAS 21
4.5 OPEN LOOP 22
4.5.1 Number of eigenmodes 22
4.5.2 Zernike polynomial production 23
4.6 CLOSED LOOP 25
4.6.1 Dependence of μ 25
4.6.2 Number of eigenmodes 26
4.6.3 Improvement 27

5 DISCUSSIONS AND CONCLUSIONS 28

6 APPENDIX 1 30

6.1 THE LEAST SQUARE METHOD 30
6.2 ZERNIKE POLYNOMIALS 31
6.3 PROGRAM SOURCE CODE 31
6.3.1 Matlab code transforming an interferogram into Zernike coefficients 31
6.3.2 Control program for the mirror 34

7 REFERENCES 36

1 INTRODUCTION

Light that propagates through a medium, for example the atmosphere, may become distorted due to wavefront perturbations. This is due to turbulence effects which introduce phase perturbations that need to be compensated. Adaptive optics is an area of science where controllable optical elements are used to improve an optical system. To narrow this description it is common to only talk about systems with a closed-loop control that works in real time[1]. An adaptive optics system also includes a wavefront sensor and a feedback control system. The science of adaptive optics has been developed since the 1960s. The main use has been high budget projects such as compensation of atmospheric turbulence in astronomical telescopes and improving the beam quality in high power lasers[2]. Lately, adaptive optics has become more available. This is due to the development of cheaper components such as e.g. membrane mirrors, bimorph mirrors and liquid crystal devices. New areas for adaptive optics are, for example, atmospheric turbulence correction of laser countermeasure systems, active imaging systems, ophthalmology and free-space optical communication[3].

The purpose of this work was to analyze a micromachined membrane deformable mirror (MMDM). In order to evaluate the mirror a transfer function was generated. The work included assembling an experimental setup for the evaluation. The mirror is commercially available from OKO Technologies in the Netherlands. This type of mirrors has been in production since 1997[4]. The specific mirror used in this study had 37 actuators that individually control different areas of the mirror surface. The mirror has a continuous surface due to the membrane structure. The spatial response of the mirror was studied to investigate how well the mirror can correct for wavefront errors. The evaluation of the mirror was done with a Zernike polynomial representation. The mirrors capability to produce wavefronts corresponding to Zernike polynomials was tested. Only the mirrors spatial domain has been investigated i.e. the response time has not been considered. Nor have any of the algorithms been optimized to work in real time.

2 THEORY

2.1 Optical waves

This section gives a brief description of the wave nature of light. Light can be described as an electromagnetic field, which propagates in time and space. To express the propagation of the light a complex field notation is often used. A scalar representation can be used and the electromagnetic field is expressed as

$$\bar{\mathbf{E}}(\bar{\mathbf{r}},t) = \bar{\mathbf{A}}\exp(\bar{\mathbf{k}}\cdot\bar{\mathbf{r}} - \omega t) = \bar{\mathbf{A}}e^{i\varphi} \tag{1}$$

where $\bar{\mathbf{E}}(\bar{r},t)$ is the electric field vector at position r and time t, A is the amplitude of the electromagnetic field, k is the wave vector with magnitude $\frac{2\pi}{\lambda}$, in vacuum (and air) which describes the propagation of the wave in space, ω is the angular frequency of the light and φ is the phase.

At the time $t = t_0$ the wave $\bar{\mathbf{E}}(\bar{\mathbf{r}},t) = \bar{\mathbf{A}}e^{i\varphi}$ consists of surfaces where the phase $\varphi = \text{constant}$. These surfaces are called wavefronts[5]. When a wave only propagates in one direction it can be described by the wave vector k. For example, if the wave propagates in the x-direction $\bar{\mathbf{k}} = k_x\hat{\mathbf{x}}$ the wave is then described as (assume that $t_0 = 0$ for simplicity)

$$\bar{\mathbf{E}}(\bar{\mathbf{r}},t) = \bar{\mathbf{A}}\exp(kx - \omega t) = \bar{\mathbf{A}}e^{i\varphi} \quad (2)$$

Then, φ = constant for all planes described by $\hat{x}$ and consequently the wave is called a plane wave (Figure 1). A wave which propagates uniformly in all directions is described by $\hat{\mathbf{k}}$ being equal in all directions. Then, the wavefront is described by a sphere and the wave is called a spherical wave. An example of a spherical wave is depicted in Figure 1. The deviation of the wavefront from a plane wave is denoted aberration.

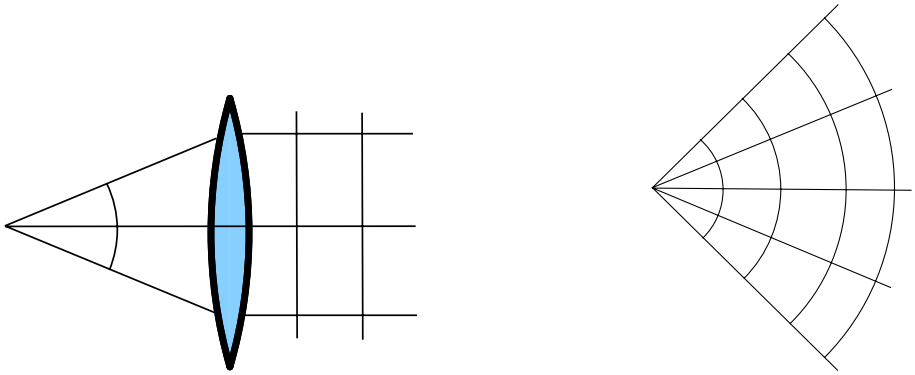

Figure 1 A plane wave created by a lens (left) and a spherical wave created by a point source (right).

2.2 Adaptive optics

An adaptive optics system consists of a wavefront sensor, a correction element and a control system. One example of a wavefront sensor is an interferometer (described in chapter 2.3) which measures the aberration of the light beam. The control system commonly uses a closed loop to determine how the correction element should compensate for the aberration.

2.2.1 The deformable mirror

In this work a deformable mirror is the active element. The principle of the deformable mirror is that after the aberration has been determined the mirror forms into a shape that cancels the aberration (in the ideal case) in the reflected beam. The principle is depicted in Figure 2.

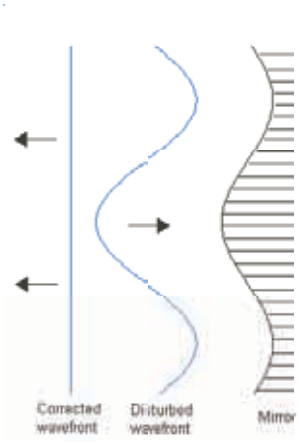

Figure 2 Principle of a deformable mirror. The mirror cancels the aberration and the reflected wave is a plane wave.

The mirror deflection $U(x,y)$ is given by Poisson's equation[6]

$$U(x,y) = -\frac{P(x,y)}{T} \tag{3}$$

where *P(x, y)* is the external load and *T* the membrane tension. In this case, *P(x, y)* is caused by electrostatic forces and is derived according to

$$P(x,y) = -\frac{\varepsilon\varepsilon_0 V_{Potential}^2(x,y)}{d^2(x,y,P)} \tag{4}$$

and *T* is given by

$$T = \frac{Eh\delta^2}{2(1-\nu)} \tag{5}$$

$V_{potential}(x,y)$ is the potential distribution on the actuator structure, $\varepsilon\varepsilon_0$ is the dielectric constant, $d^2(x,y,P)$ is the distance between the membrane and the actuator structure, *E* is Young's modulus of the membrane material, *h* is the thickness of the membrane, ν is the Poisson ratio of the membrane material and δ is the in-plane membrane elongation due to the stretching. Combining equations (3) to (5), yields that the deflection of the mirror is proportional to the square of the voltage i.e. $U(x,y) \propto V^2$.

2.3 Interferometry

When two light beams overlap the sum of the beams depends on both the amplitude and the phase. If they have the same phase constructive interference and a high intensity is produced. If the two beams are out of phase, on the other hand, they produce a destructive interference and the intensity becomes zero. An instrument that uses the optical differences between two light beams to produce an interference pattern is called an interferometer.

2.3.1 The principle of a Michelson interferometer

A schematic drawing of a Michelson interferometer is shown in Figure 3. From the light source, a beam (represented by a plane wave) falls on the beam splitter (BS) which divides the light into two paths. The two beams are reflected on the mirrors M1 and M2, respectively. The beams are subsequently summed into one beam which is examined in the detector. Because of the different optical paths the two beams experience they can be out of phase with each other. This can be due to the mirrors, or a component in one of the arms, causing a change in the optical path length. If the difference in path length between the mirrors is denoted *d*, $\Delta = 2d$ is the optical path length difference between the two beams. Hence, $\Delta = m\lambda$ gives constructive interference, while $\Delta = (m+1/2)\lambda$ gives destructive interference (λ is the wavelength).

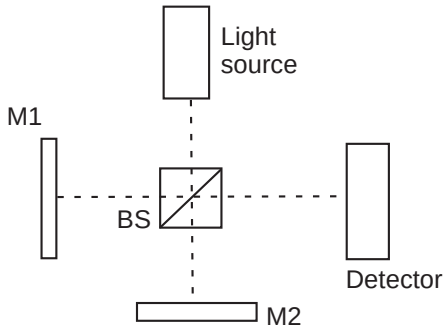

Figure 3 Schematic drawing of a Michelson interferometer

2.3.2 Interferogram

The registered interferometric pattern is called an interferogram. The interferogram can be described mathematically by the intensity of the electrical field. By definition the intensity is proportional to the square of the absolute value of the complex field of the wave. If E_1 and E_2 represent the electric fields of the light beams the intensity can be calculated as follows

$$I \propto \left|E_1 + E_2\right|^2 = \left|E_1\right|^2 + \left|E_2\right|^2 + E_1E_2^* + E_1^*E_2 = \\ I_1 + I_2 + I_{12} \tag{6}$$

Using the complex representation of a wave, $E = Ae^{i\varphi}$, the intensities in equation (6) can be written as

$$\begin{aligned} I_1 &= \left|A_1e^{i\varphi_1}\right|^2 = A_1^2 \\ I_2 &= \left|A_2e^{i\varphi_2}\right|^2 = A_2^2 \\ I_{12} &= A_1e^{i\varphi_1}A_2e^{-i\varphi_2} + A_1e^{-i\varphi_1}A_2e^{i\varphi_2} = \\ &= A_1A_2\left(e^{i(\varphi_1-\varphi_2)} + e^{-i(\varphi_1-\varphi_2)}\right) = A_1A_2\,2\cos\left(\varphi_1-\varphi_2\right) \\ &= \sqrt{I_1I_2}\,2\cos\left(\varphi_1-\varphi_2\right). \end{aligned} \tag{7}$$

Note that A_i is a real number. Constructive interference is observed when $\cos(\varphi_1-\varphi_2) = 1$ and destructive interference when $\cos(\varphi_1-\varphi_2) = -1$. If $I_1 = I_2 = I$ we obtain

$$I_{\max} = 2I + 2I = 4I \\ I_{\min} = 2I - 2I = 0 \tag{8}$$

Studying interferogram dark and bright fringes can be observed. The phase difference between a dark and a bright fringe is a half wavelength, $\lambda/2$. Two examples of interferograms are presented in Figure 4. In the left interferogram one of the beams is tilted giving rice to vertical stripes. In the right figure one of the beams has a spherical aberration generating concentric circles.

2.3.3 Fourier transform analysis of interferogram

The Fourier transform method for analyzing fringe patterns in the interferograms was first developed by Takeda et al. in 1981[7]. The method uses a carrier frequency f_0 which is achieved by tilting the reference beam. The interferogram is described by

$$g(x,y) = a(x,y) + b(x,y)\cos(2\pi f_0x + \phi(x,y)) \tag{9}$$

where $a(x,y)$ and $b(x,y)$ are variations in the intensity due to errors in the interferometer such as uneven reflections etc. The desired information is obtained by considering the phase, $\phi(x,y)$. It is important that $\phi(x,y)$ varies slowly compared to f_0, so that $\phi(x,y)$ can be easily separated from the added phase f_0. If they are mixed, the tilt component in the interferogram must be increased. Now the fringe pattern can be rewritten as

$$g(x,y) = a(x,y) + c(x,y)\exp(i2\pi f_0x) + c^*(x,y)\exp(-i2\pi f_0x) \tag{10}$$

where

$$c(x,y) = \frac{1}{2} b(x,y) \exp(i\phi(x,y)) \tag{11}$$

The two dimensional Fourier transform is given by

$$G(f_x, f_y) = A(f_x, f_y) + C(f_x - f_0, f_y) + C^*(f_x + f_0, f_y) \tag{12}$$

where $A(f_x, f_y), C(f_x - f_0, f_y)$ and $C^*(f_x + f_0, f_y)$ denote the energy spectra of the interferogram after the Fourier transform operation. An example of this method is illustrated in Figure 5. The analyzed interferogram consisted of the added tilt (f_0) and a defocus aberration(Figure 5A). The absolute value of the Fourier transform of the interferogram (i.e. the energy spectrum) is shown in Figure 5 b.

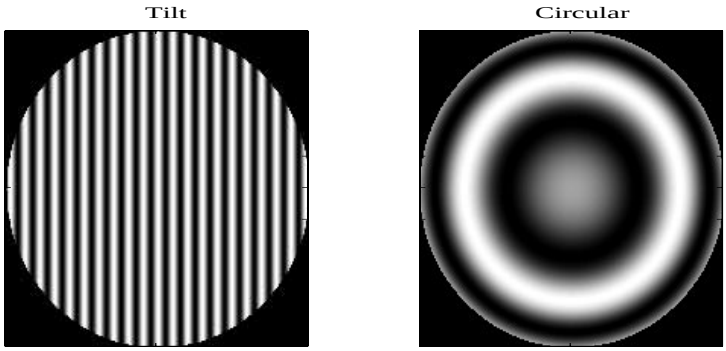

Figure 4 Interferograms with tilted (left) and spherical aberrations (right). The interferograms were simulated using the software package LightPipes for Matlab.

The left white spot in the Fourier transform corresponds to $C(f_x\text{-}f_0,f_y)$, the spot in the middle is the DC component $A(f_x,f_y)$ and the spot to the right is $C(f_x+f_0,f_y)$. The desired information $\phi(x,y)$ is now stored in $c(x,y)$. In this example, f_0 is large enough so $C(f,y)$ can be separated by translating the Fourier transform $G(f_x,f_y)$ with the distance f_0 along the f_x-axis and then use a window function to filter $C(f_x,f_y)$. Figure 5c shows the translated and filtered Fourier transform. Only $C(f,y)$ is present in the picture. To obtain $c(x,y)$, which contains the phase information, the inverse Fourier transform of $C(x,y)$ is calculated. To determine the phase $\phi(x,y)$ the complex logarithm of $c(x,y)$ is subsequently calculated as

$$\begin{aligned} &\mathbf{F}^{-1}\{C(f,y)\} = c(x,y) \\ &\log(c(x,y)) = \log(\frac{1}{2} b(x,y) + i\phi(x,y)) \end{aligned} \tag{13}$$

The phase values derived from the inverse Fourier transform are within a domain between $-\pi$ and $+\pi$. The real phase, however, often occupy a larger domain. To compensate for this behaviour $\phi(x,y)$ must be unwrapped. The phase map corresponding to the spherical aberration (defocus) is displayed in Figure 5d.

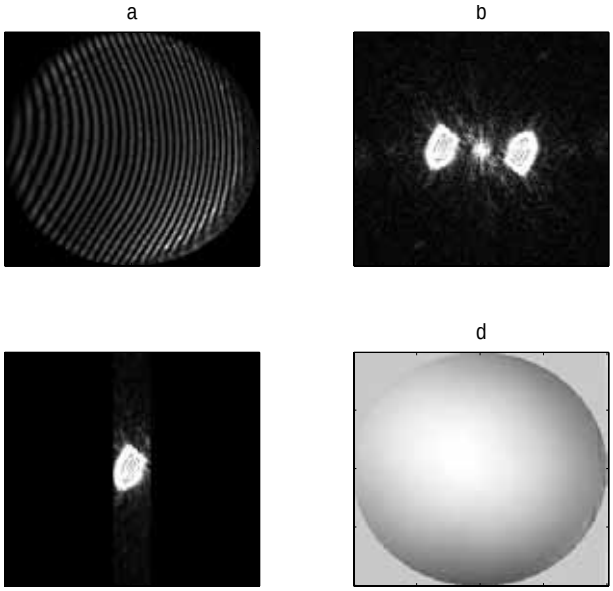

Figure 5 a) An interferogram consisting of tilt and spherical terms. b) The Fourier transform of the interferogram (energy spectrum). c) The translated and filtered Fourier transform corresponding to $C(f_x,f_y)$. d) The extracted phase after an inverse Fourier transform.

2.3.4 Quick Fringe

The program Quick Fringe was used as an alternative method to analyze interferograms[8]. Quick Fringe works best with about ten fringes to analyze. To achieve this a tilt term is added to the reference beam by tilting one of the interferometer mirrors. Since the introduced tilt is known it can easily be removed in the fringe analyzes. Quick Fringe uses linear regression to find the Zernike polynomials which are used to reconstruct the wavefront (see section 2.4 for information on Zernike polynomials). The ability to remove optical aberrations such as tilt, defocus, coma and astigmatism is a functionality of the program. Even if this option is used the Zernike coefficients produced by the program are not affected since the removal of optical aberrations are only shown in the images produced by the program[8]. Hence, this fact limited the applicability of using Quick Fringe for interferogram analyzes. Instead the Fourier transform method described above was used in the characterization of the deformable mirror.

2.4 Zernike polynomials

The notations used in this chapter are the same as those presented in ref[9]. Zernike polynomials define a two dimensional basis and are commonly used to describe aberrations. They are especially useful in describing the de-composition of a wavefront having a circular aperture. The wavefront can then be represented by the coefficients in a linear combination of Zernike polynomials. Zernike polynomials have the following properties:

1. They are orthogonal over the unit circle, i.e. $\int_0^1 \int_0^{2\pi} Z_n(\rho,\theta) Z_{n'}(\rho,\theta)\,\rho\, d\rho\, d\theta = \delta_{nn'}$
2. They have simple rotational symmetry, which means that all polynomials can be written as a product $z(\rho,\theta) = R(\rho)G(\theta)$
3. The angular function, $G(\theta)$, is continuous and periodic with period 2π and can be written as $G(\theta) = e^{\pm im\theta}$
4. The radial function, $R(\rho)$, is a polynomial of degree n and has no power less then m
5. If m is even, $R(\rho)$ must be even, and if m is odd, $R(\rho)$ must be odd

6. R_n^m are orthogonal functions i.e. $\int_0^1 R_n^m R_{n'}^m \rho d\rho = \frac{\delta_{nn'}}{2(n+1)}$

and finally *R(1) = 1*.

A special case of Jacobi polynomials fulfil properties 4 to 7. We use the help function *Q* so that

$$R_{2n-m}^m(\rho) = Q_n^m(\rho)\rho^m \tag{14}$$

where *Q* is a polynomial of order *2(n- m)* and can be written as

$$Q_n^m(\rho) = \sum_{s=0}^{n-m}(-1)^s \frac{(2n-m-s)!}{s!(n-s)!(n-m-s)!}\rho^{2(n-m-s)} \tag{15}$$

.

Here, ρ is the distance from origin and θ is the angle from the *x*-axis. The first 37 Zernike polynomials are presented in Appendix1. Some of the first polynomials are shown in Figure 6. Note that this is not the only way to number Zernike polynomial. The reason for using this numbering of the polynomials is to use the same numbering as in Quick Fringe[8].

2.5 Description of the mirror surface

Instead of calculating the mirror surface the wavefront from the reflected beam is determined. The mirror surface corresponds to half of the magnitude of the wavefront. The wavefront can be described as a vector of Zernike coefficients, with the Zernike polynomials as a base. The fitting of the polynomials can be carried out numerically with e.g. Matlab using the least square method (see Appendix1).

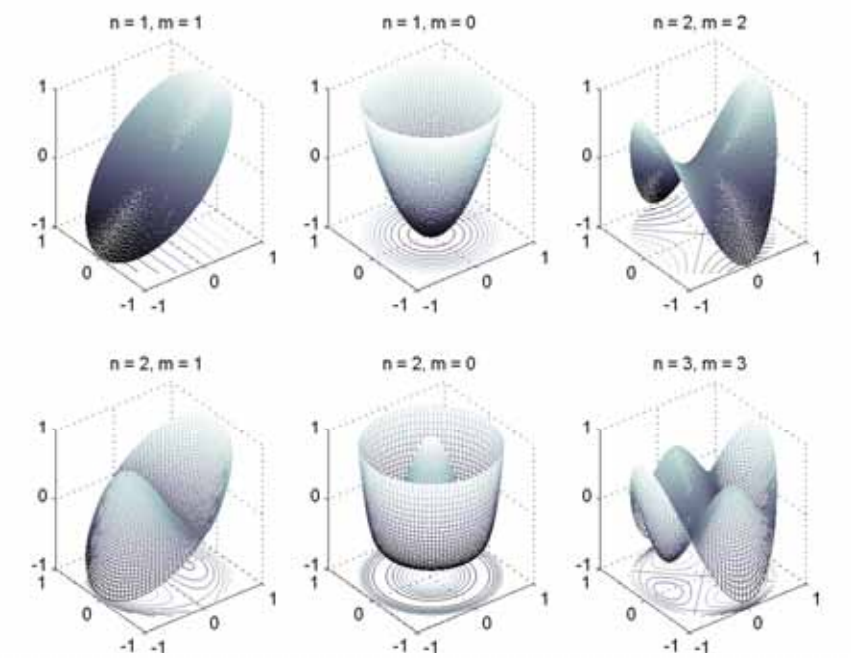

Figure 6 Example of Zernike polynomials.

The wavefront can be described according to

$$\phi(x,y) = \sum_{k=1}^{M} a_k z_k(x,y) + \varepsilon \tag{16}$$

where a_k denotes the Zernike coefficients and $z_k(x,y)$ the Zernike polynomials, respectively. ε is the error due to the fact that only M Zernike polynomials are used. This error is ignored below in the description of the mirror surface. Applying voltage to the mirror actuators causes the surface of the membrane to change. The deflection of the surface is proportional to the square of the applied voltage as pointed out above [10,11]. The shape of the deflection, applying a voltage to one actuator is denoted the influence function of the actuator. A three dimensional plot of an influence function is shown in Figure 7.

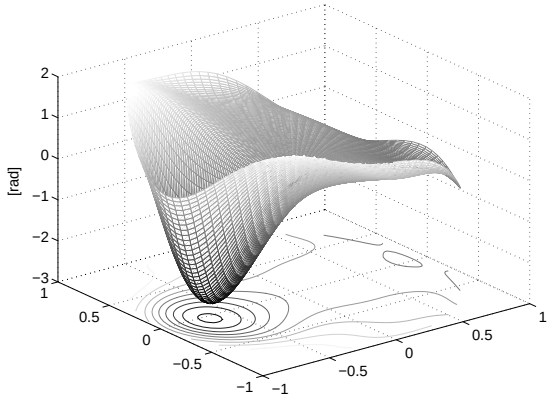

Figure 7 Example of an influence function. In this case 200V was applied to actuator number 8.

The surface shape can now be described as

$$\phi(x,y) = \phi_0(x,y) + \varphi_l(x,y)c_l \tag{17}$$

where c_l is a control signal for actuator l and $\phi_0(x,y)$ is the initial shape of the mirror surface. The control signal is proportional to the square of the applied voltage. φ_l is the response function, which describes how the mirror deforms with a voltage applied on actuator l. Assuming that the deformation can be described as a linear superposition of the deformation from single actuators the deflection of the mirror surface can be expressed as

$$\phi(x,y) = \phi_0(x,y) + \sum_{l=1}^{P} \varphi_l(x,y)c_l \tag{18}$$

where P is the number of actuators. Expanding the different response functions $\varphi(x,y)$ into Zernike polynomials we get

$$\varphi_l(x,y) = \sum_{k=1}^{M} r_{kl} z_k(x,y) \tag{19}$$

Equations (18) and (19) gives

$$\Delta\phi(x,y) = \phi(x,y) - \phi_0(x,y) = \sum_{l=1}^{P} c_l \left(\sum_{k=1}^{M} r_{kl} z_k(x,y) \right) = \sum_{l=1}^{P} \left(\sum_{k=1}^{M} c_l r_{kl} \right) z_k(x,y) \tag{20}$$

Another way to express equation (20) is to let $\bar{\mathbf{\Phi}}$ describe the Zernike coefficients of the mirror surface i.e. the vector of a_k in eq. (16). Collect r_{kl} into the matrix $\boldsymbol{R}$ and the control signals of all the actuators into the vector $\bar{\mathbf{c}}$ [10]. The equation that relates the applied actuator voltage into the deformation of the mirror surface then becomes

$$\Delta\mathbf{\Phi} = \mathbf{R}\bar{\mathbf{c}} \;\; \Delta\bar{\mathbf{\Phi}} = \mathbf{R}\bar{\mathbf{c}} \tag{21}$$

The matrix $\boldsymbol{R}$ is called the transfer function and describes the response of the deformable mirror. The transfer function matrix is of the size $M \times P$ i.e. in general not a square matrix.

2.6 Reconstruction of the wavefront

To reconstruct the wavefront we need to calculate the vector of control signals required to produce the desired wavefront. An inversion of the equation (21) is needed to accomplish a reconstruction scheme. However, since $\mathbf{R}$ is not a square matrix it is not possible to calculate the inverse. Instead Singular Value Decomposition (SVD) is used to calculate a pseudo-inverse. Singular value decomposition breaks up a matrix in three matrices. Using SVD, $\boldsymbol{R}$ can be expanded as[12]

$$\mathbf{R} = \mathbf{U}\mathbf{\Lambda}\mathbf{V}^T \,. \tag{22}$$

These three matrixes have different properties[13]. $\boldsymbol{U}$ and $\boldsymbol{V}$ are orthogonal matrices. The columns of $\boldsymbol{U}$ describes the eigenmodes of the mirror whereas the columns of $\boldsymbol{V}$ describes the eigenmodes of the control signals. $\mathbf{\Lambda}$ is a diagonal matrix where the diagonal values i are the eigenvalues. These eigenvalues relates the column vector $\boldsymbol{u}_i$ to the column vector $\boldsymbol{v}_i$. The following assumptions are made in the SVD scheme:

- If $\lambda_i = 0$ the mode $\boldsymbol{u}_i$ is not correctable and the control signal $\boldsymbol{v}_i$ has no effect on the mirror
- If $\lambda_i \neq 0$ the mode $\boldsymbol{u}_i$ is correctable.

The magnitude of λ_i determines the sensitivity of the mode. High values of λ_i are favourable, because they bring less noise to the transfer function. The inverse of $\boldsymbol{R}$ is denoted $\mathbf{C}$ and obtained as

$$\mathbf{C} = \mathbf{V}\mathbf{\Lambda}^{-1*}\mathbf{U}^T \tag{23}$$

where $\mathbf{\Lambda}^{-1*}$ is the pseudo-inverse or the least-square inverse. The pseudo-inverse is formed by transposing $\mathbf{\Lambda}$ and replacing the nonzero λ_i with the inverse λ_i^{-1}. To eliminate the noise contributions the smallest values of λ_i are set to zero.

2.7 Wavefront error

One way to measure the wavefront quality is to use the root mean square (rms) error. The rms error is also commonly denoted the standard deviation and is defined as

$$rms = \sqrt{\int_0^1 \int_0^{2\pi} \left(\Phi(\rho,\theta) - \langle\Phi(\rho,\theta)\rangle\right)^2 \rho d\rho d\theta} \,. \tag{24}$$

This expression can be simplified by dividing $\Phi(\rho,\theta)$ into normalized Zernike coefficients. To normalize the Zernike polynomial the normality factor n_k is used. The normality factor is calculated according to

$$n_k^2 = \int_0^1 \int_0^{2\pi} \left(z_k^2 \rho d\rho d\theta\right) \,. \tag{25}$$

If all the Zernike polynomials are normalized they are orthonormal i.e.

$$\int_0^1 \int_0^{2\pi} (n_k z_k)(n_l z_l)\rho d\rho d\theta = \delta_{kl} \tag{26}$$

If we use the fact that the first polynomial equals the mean of the wavefront $a_0 n_0 z_0 = \langle \Phi(\rho,\theta) \rangle$ the rms can be rewritten as

$$rms = \sqrt{\int_0^1 \int_0^{2\pi} \left(\Phi(\rho,\theta) - \langle \Phi(\rho,\theta) \rangle \right)^2 \rho d\rho d\theta} = \sqrt{\int_0^1 \int_0^{2\pi} \left(\sum_0^\infty a_k n_k z_k - a_0 n_0 z_0 \right)^2 \rho d\rho d\theta} = \\ = \sqrt{\left(\sum_1^\infty a_k n_k z_k \right)^2} \tag{27}$$

Consequently the wavefront rms can be expressed in terms of the Zernike coefficients a_k.

The Strehl ratio is another way to measure the error of the wavefront. The Strehl ratio is defined as the ratio between the on-axis intensity of an aberrated beam and an unaberrated beam. In presence of a tilt term the on-axis aberration is defined as the normal to the plane of the tilt. Due to this fact tilt errors should be removed when calculating the Strehl ratio. The Strehl ratio is written as

$$S = \frac{1}{\pi^2} \left| \int_0^1 \int_0^{2\pi} e^{ik\Phi(\rho,\theta)} \rho d\rho d\theta \right|^2 \tag{28}$$

where $\Phi(\rho,\theta)$ is the aberrated wavefront. The Strehl ratio is a value between zero and one where a higher Strehl ratio corresponds to a better performing system[1]. The Strehl ratio can also be expressed in terms of the rms if the unit of the rms error is in radians

$$S \approx e^{-rms^2} . \tag{29}$$

This is an approximate expression but if the Strehl ratio is larger then 0.6 the error is less then 10%[14].

3 EXPERIMENTAL METHODS

3.1 Experimental setup

The experimental setup consists of two main parts; the interferometer and the control system. The deformable mirror is a part of the interferometer.

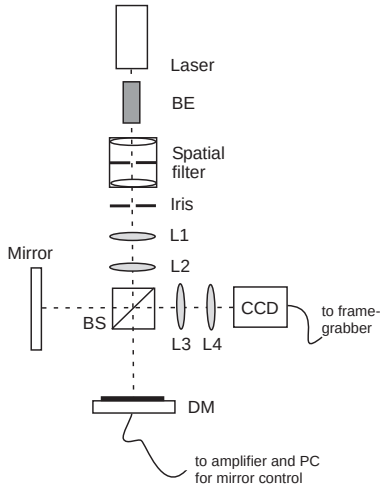

Figure 8 Schematic drawing of the interferometer setup. BE: beam expander, BS: beam splitter, DM: deformable mirror, L: lenses, CCD: camera.

3.1.1 The interferometer

The interferometer setup is shown Figure 8 and Table 1 specifies values for some of the used components. The laser beam is directed through a beam expander and a spatial filter consisting of a microscope lens and a pin hole.

Table 1 Parameters of the interferometer setup

Item	Description
Laser	*HeNe, λ = 633 nm*
L1	*f = - 50 mm*
L2	*f = 150 mm*
L3	*f = - 50 mm*
L4	*f = 100 mm*
CCD	Resolution 1040x1160, 12 bits 1/60 s shutter duration

The low-pass spatial filter improves the beam quality. After the spatial filter the beam size is reduced with an iris. If the diameter is too small it causes diffraction fringes. The iris is kept large enough to avoid this problem. Two lenses are added to make the light beam collimated (i.e. represent a plane wave). The beam passes through a beam splitter, which divides it into two parts. One beam falls onto the deformable mirror and the other falls onto the reference mirror. Both the deformable mirror and the reference mirror holders can be tilted. To obtain an extra tilt pattern for the Fourier transform method (see chapter 2.3.3) the reference mirror is tilted so that there is approximately 70 fringes on the interferogram. After the beam splitter the light passes through two lenses in order to adapt the beam to the detector in the CCD-camera. The interferogram is captured by the CCD-camera and transferred to a PC using a frame grabber card. A photograph of this setup is shown in Figure 9.

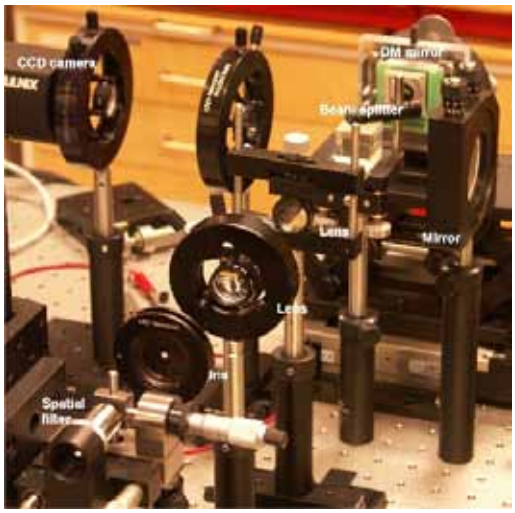

Figure 9 Experimental setup showing the interferometer and the deformable mirror.

3.1.2 The control system

The mirror is controlled using two PCI-cards (D/A converters) installed on an ordinary computer. One card controls the inner 19 actuators and the other card controls the outer 18 channels. The two cards worked in different ranges. One worked between 0 to 215 V and the other in the range 0 to 613 V (after being amplified). Both cards have eight bit resolution. This means that the card that operates between 0 to 215 V has a higher resolution in the mirrors working area. This card was used for the inner 19 actuators because these are assumed to affect the mirror the most. The PCI cards are connected to amplifiers, which amplifies the signal 59 times. A drawing of the amplifier with inputs and outputs is shown in Figure 10. The driving voltage of the amplifier is ±15 V. There is also an input that controls the maximum voltage output from the amplifiers. The maximum voltage of the mirror is 215 V. To have a security margin the maximum output voltage of the amplifiers was set to 200 V.

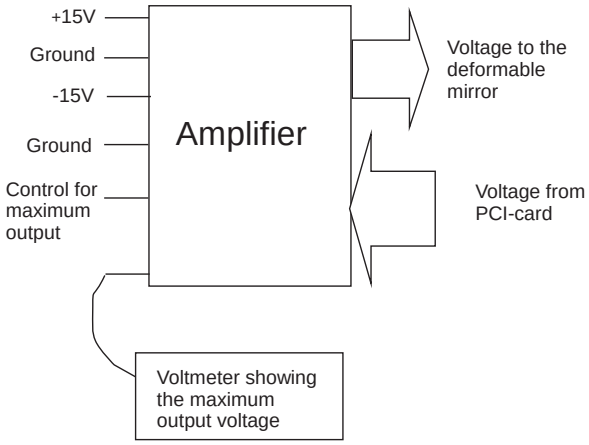

Figure 10 Schematic drawing of the amplifier

3.1.3 Technical details – the deformable mirror

The micromachined deformable mirror (MMDM) used in this study is produced by OKO Technologies in the Netherlands [4]. The diameter of the mirror is 15 mm and the active area is 12 mm. It can be manipulated with 37 actuators that are positioned according to Figure 11. When a voltage is applied to one of the actuators the mirror moves toward the actuator structure

taking a concave shape. The maximum peak to valley distance for the mirror is about 7 μm[15]. The maximum voltage for the examined mirror was 215 V.

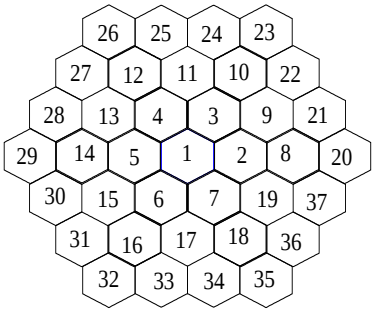

Figure 11 Actuator structure.

The mirror consists of two major parts; the actuator structure and the flexible membrane mirror. The flexible membrane is mounted with a 20 to 100 μm gap relative to the actuator structure. The mirror is formed by the 0.5 μm thick silicon nitride membrane which is coated with a 0.2 μm evaporated layer of aluminium to make the membrane reflective[16]. The principle of the mirror is shown in Figure 12. The maximum number of modes is obtained by using approximately 62% of the mirrors area which corresponds to 9.3 mm[17]. In the captured image used for interferogram analysis the square regime that contains the beam from the deformable mirror was extracted. Subsequently, 62% of this square was cut out and a circular aperture was exported to Matlab. This image was then used in the analysis.

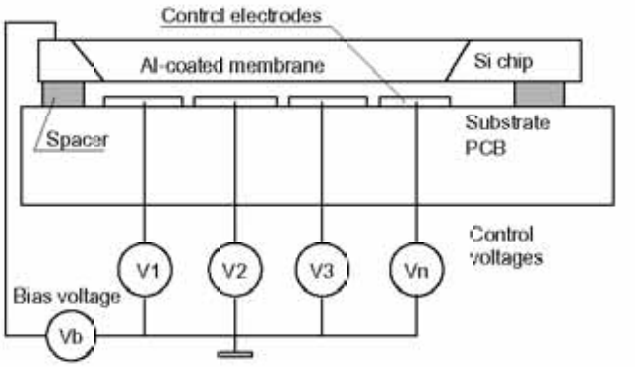

Figure 12 Schematics of the micromachined deformable membrane mirror.

3.2 Determining the transfer function

The theory of the transfer function was presented in chapter 2.5. The mirror surface $\bar{\Phi}$ is described by

$$\bar{\Phi} = \mathbf{R}\bar{\mathbf{c}} + \bar{\Phi}_0 \tag{30}$$

or

$$\begin{pmatrix} \phi_1 \\ \phi_2 \\ \vdots \end{pmatrix} = \begin{pmatrix} r_{1,1} & r_{1,2} & \cdots \\ r_{2,1} & r_{2,2} & \cdots \\ \vdots & \vdots & \ddots \end{pmatrix} \begin{pmatrix} c_1 \\ c_2 \\ \vdots \end{pmatrix} + \begin{pmatrix} \phi_{1,0} \\ \phi_{2,0} \\ \vdots \end{pmatrix} \tag{31}$$

In order to determine the transfer function ***R*** the voltage was varied for one actuator at the time. The voltage was set to eight different values ranging from 44 to 184 V chosen so that the squares of the values increase with a constant. The reason to have equal distance between the square of the voltages is that the mirror deflection is proportional to the voltage squared. The other actuators were kept at a constant voltage, V_{bias}. Using LabView the interferograms were recorded and saved. Subsequently they were analyzed (using Matlab) and the Zernike coefficients were calculated. This was done for all 37 actuators leading to 37x8 interferograms. When all the actuators are set to V_{bias} the mirror forms into a bias shape. The control signal ***c*** was set to zero for V_{bias}. To avoid numerical problems with large values of c, the vector ***c*** was normalized using the maximum actuator voltage allowed for the mirror. Due to the fact that the mirror deformation is proportional to the square of the applied voltage ***c*** should also be proportional to the square of the voltage suggesting the following normalization.

$$c = \left(V^2 - V_{bias}^2\right)/200^2 . \tag{32}$$

The measurements were preformed by keeping $c_i = 0$ for all the actuators except for one, c_j, reducing equation (3.1) to

$$\begin{pmatrix} \phi_1 \\ \phi_2 \\ \vdots \end{pmatrix} = \begin{pmatrix} r_{1,j} \\ r_{2,j} \\ \vdots \end{pmatrix} \begin{pmatrix} c_1 \\ c_2 \\ \vdots \end{pmatrix} + \begin{pmatrix} \phi_{1,0} \\ \phi_{2,0} \\ \vdots \end{pmatrix} . \tag{33}$$

The Zernike polynomials that were used were the last 34 of the 37presented in Appendix1. The first three (piston and tilt) were not used in the transfer function. Piston does not affect the phase of the light and the tilt component is easier to compensate with an additional tip-tilt mirror. There were 37 equations (one for each actuator) to be solved. Each one can be solved using the least square method where $r_{i,j}$ and c_j are obtained. $\phi_{0,j}$ are obtained for each of the 34 equations. Note that all these 34 $\phi_{0,j}$ are nearly identical (where j is the number of the actuator). $\bar{\mathbf{\Phi}}_0$ corresponds to the mirror surface with V_{bias} applied to all the actuators. For one of the measured transfer functions the standard deviation of the coefficients was less then or equal to 0.013 rad. The highest standard deviation was obtained for polynomial number three, where the coefficient value was -13.62 rad. The average of the different $\phi_{0,j}$ was calculated and used as $\bar{\mathbf{\Phi}}_0$.

3.3 Mirror control

The two main ways to control the mirror is by using an open or a closed loop scheme. With an open loop a desired wavefront is produced using only the transfer function. The open loop control signal is calculated by inverting the transfer function as defined in eq. (23). As stated in chapter 2.6, **R** can not always be inverted. Instead the pseudo inverse is calculated using singular value decomposition. The inverse is denoted **C**. The wanted wavefront, Φ_{wanted}, was chosen and the vector or control signals were calculated using

$$\bar{\mathbf{c}} = \bar{\mathbf{c}} + \mu\mathbf{C}\left(\bar{\mathbf{\Phi}}_{wanted} - \bar{\mathbf{\Phi}}_{bias}\right) \tag{34}$$

As with the open loop scheme **C** is calculated and $\bar{\mathbf{\Phi}}_{wanted}$ is chosen in the closed loop scheme. By modifying eq. (34) the closed loop scheme is obtained according to

$$\bar{\mathbf{c}}_n = \bar{\mathbf{c}}_{n-1} + \mu\mathbf{C}\left(\bar{\mathbf{\Phi}}_{wanted} - \bar{\mathbf{\Phi}}_{n-1}\right) \tag{35}$$

μ is a number between 0 and 1. The optimal value of μ is determined by experiment. The closed loop iteration starts with an open loop correction to determine $\bar{\mathbf{c}}_0$ and $\bar{\mathbf{\Phi}}_0$.

3.4 Zernike polynomial production

Experiments were carried out to see how well the mirror can produce different Zernike polynomials. The main experiments were performed using an open loop scheme and then in some of the experiments a closed loop was utilised. Using the open loop scheme one coefficient at the time of $\bar{\mathbf{\Phi}}_{wanted}$ was varied while the others were kept at zero. Zernike polynomial production was performed in different ways:

1. with a flat surface as a bias. The transfer function was measured with V_{bias} taken to be 100, $100/\sqrt{2}$ and 152 V and $\Phi_{wanted}(x,y) = a_k z_k(x,y)$

2. with a bias having a constant voltage applied on all the actuators. V_{bias} was used as 100, $100/\sqrt{2}$ and 152 V and $\Phi_{wanted}(x,y) = \Phi_{bias} + a_k z_k(x,y)$

3. with a spherical bias $\Phi_{bias}(x,y) = -14 z_3(x,y)$ rad.

The reason to use a bias is that the mirror only deforms towards the actuator structure. With a bias that has a constant voltage applied to all the actuators, as in case 2 above, the dynamic range of the mirror should increase. The drawback of using this procedure is that aberrations are introduced to the system. The bias $100/\sqrt{2}$ V was evaluated because it theoretically corresponds to half of the maximum deflection. When measuring the peak to valley (PV) distance of the mirror detection the half of the maximum deflection occurs with a bias of 152 V (see chapter 4.4). The bias of 100 V was used to investigate if it is important to be in the central part working region of the mirror.

With a spherical bias that lies in the central part of the working region of the mirror the effect should be similar to applying a bias of constant voltage. The difference is that by using this transfer function to compensate for an aberration the resulting beam will be a spherical wave that can be compensated by a lens. To obtain an optimized bias the voltage to achieve this surface was obtained by using a closed loop. The transfer function with bias 152 V was used and the iteration was performed 30 times with $\mu = 0.5$. As stated in chapter 2.6 some of the eigenmodes can be set to zero in order to decrease to noise. In order to see how the result depends of the number of eigenmodes 12, 16, 20 and 25 modes were corrected when producing the Zernike polynomials.

To investigate how the results improves if we close the loop and improve the surface step by step Zernike polynomial production was preformed with polynomial three, four and eight (defocus, astigmatism and spherical aberration). These polynomials were chosen because they were easiest (three and four) and hardest (eight) to produce using an open loop scheme. The objective was to find out how the result could be improved. The μ values used were 0.3, 0.5 and 1, respectively. The iteration was stopped if the rms value of Φ_{error} was lower then 0.2 rad or after 16 iterations. As for the open loop the Zernike polynomials were produced using 12, 16, 20 and 25 eigenmodes. The bias used for closed loop experiments was the spherical bias.

4 RESULTS

4.1 Validity of the Fourier transform method

To compare the developed Matlab script using the Fourier transform method and Quick Fringe, an interferogram was analyzed using the different methods. The analyzed interferogram was

corresponding to the mirror with zero voltage on the actuators. The difference between the results comparing the methods is a constant factor. After normalizing the polynomials (dividing all the coefficients by the largest absolute value of the coefficients) the magnitude of the coefficients is similar (Figure 13). The piston and tilt coefficients are not compared. Hence, these results support the validity of the Fourier transform method used throughout this work.

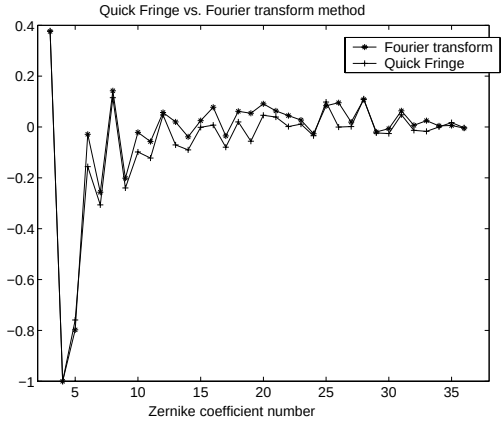

Figure 13 Quick fringe vs. the Fourier transform method. Zernike coefficients calculated from the same interferogram using Quick fringe and the Fourier transform method. Both graphs are normalised.

4.2 Linearity of the mirror

The method described in section 3.2 requires that each one of the Zernike polynomials must be linear with respect to the square of the applied voltage. To verify this assumption the Zernike polynomials were plotted versus the control signal. Note that the control signal is not the same as the applied voltage. The coefficients for Zernike polynomials number 3 and 4 are plotted versus the control signal on actuator 1 and polynomials number 14 and 15 are plotted versus the control signal on actuator 11 (Figure 14). The lines plotted together with the measurements are the results from the least square calculations verifying that the mirror response is linear. Results for other actuators, Zernike polynomials and biases were found to be similar to those presented in Figure 14.

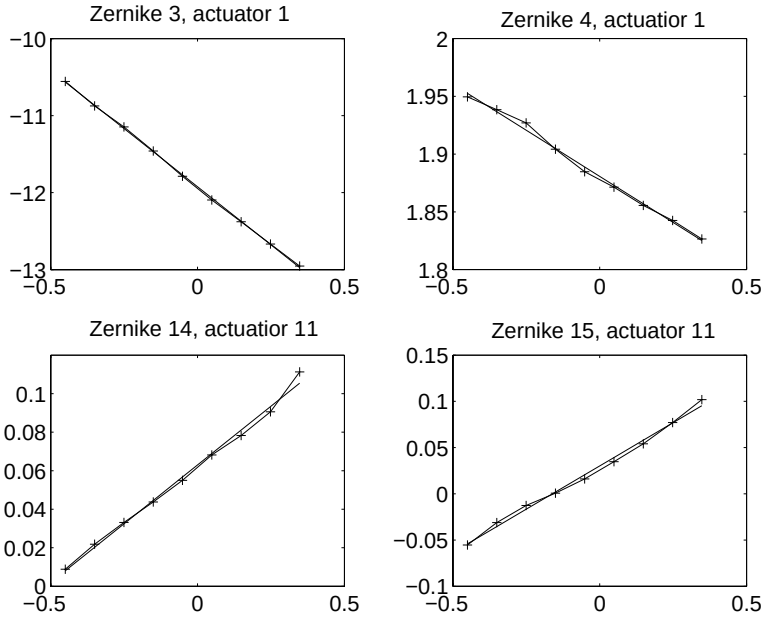

Figure 14 The mirrors Zernike coefficients (in radians) versus the control signal. The measurements are performed using the transfer function with V_{bias} = 141 V.

4.3 The eigenmodes of the mirror

Using singular value decomposition (SVD) the matrix ***U*** represents the eigenmodes of the system. Figure 15 contains the first 9 eigenmodes of the mirror with the transfer function having a 141 V bias. The modes are ordered by the magnitude of the eigenvalues λ. The figure shows that a higher number of the mode corresponds to a more complex surface.

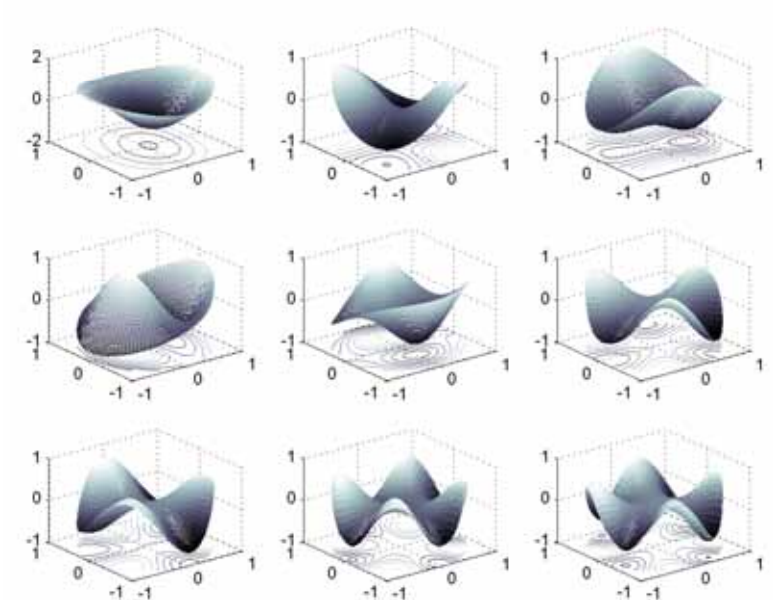

Figure 15 The first nine eigenmodes of the mirror (V_{bias} = 141 V)

4.4 Determining the bias

The total response of the mirror was measured when the same voltage was applied to all of the actuators. The wavefront peak to valley distance (i.e. the difference between the highest and lowest point on the wavefront) is depicted in Figure 15. The mirror PV distance is half of these values. The maximum PV distance was 66.4 rad corresponding to the distance 6.7 μm at the wavelength λ = 632 nm. This value does not correspond to the stated maximum deflection of 7 μm because only 62 % of the inner part of the mirror is used. The half of this distance occurs when the voltage is approximately 152 V to be compared with the theoretical value $200\,V/\sqrt{2} \approx 141\,V$.

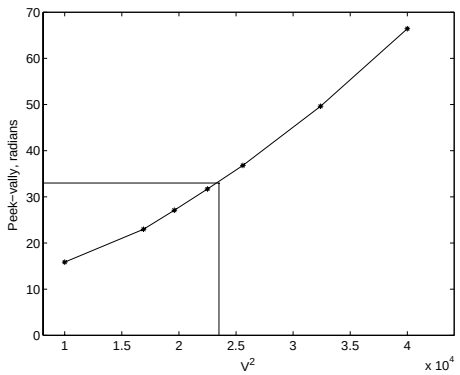

Figure 16 Peak to valley distance in radians versus the voltage squared.

4.5 Open loop

Open loop correction was used to find the optimal number of correction modes and to investigate how well the mirror could produce different Zernike polynomials.

4.5.1 Number of eigenmodes

In order to find out the optimal number of eigenmodes, 12, 16, 20 and 25 modes were used to produce different Zernike polynomials. The results varied between the tested Zernike polynomials. For some Zernike polynomials the optimal number of modes depends on the coefficient value. One example of this behaviour is shown in Figure 17. The rms value of the error is plotted versus the number of modes. The wanted surface was $\Phi_{wanted} = a_{13} \cdot z_{13}$. If a_{13} is less than -5 then 12 to16 modes is the best choice. However, when a_{13} is between -3 and -1 then 20 to 25 modes turn out to be better choice. It was not possible to find any correspondence between how easy the polynomial was to produce and the optimal number of modes. For other Zernike polynomials the experimental results showed a varying number of optimal modes.

Table 2 Optimal number of modes. The statistics show the best number of modes producing single Zernike polynomials. The utilised voltages are indicated.

	100 V	**141 V**	**152 V**	∑
12-16 modes	2	2	2	6
20-25 modes	3	3	3	9
Different	1	3	1	5
No difference	3	1	4	5

From 30 measurements, 10 polynomials with 3 different bias some statistics are shown in Table 2. "Different" means that for the same Zernike polynomial, it depends on the coefficient if it is preferable to use 12-16 modes or 20-25modes. "No difference" means that the results are independent of the number of modes. If a choice is made from these measurements 20 modes seems to be the best choice. However, more measurements are required to confirm the optimal number of modes.

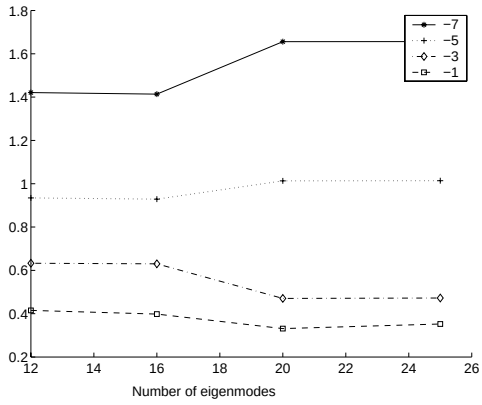

Figure 17 Dependency of the rms value as the function of different number of eigenmodes. The following values were used: $\Phi(\theta,\rho) = \Phi_{bias} + a_{13}z_{13}$ with a_{13} = -7, -5, -3 and -1 rad. The plot shows the rms value for the resulting wavefront for different number of modes.

4.5.2 Zernike polynomial production

To evaluate the open loop Zernike polynomial production the Zernike coefficients were used. They were measured using approximately 62 % of the mirror surface with the interferometer described above. The measured experimental wavefront was compared with the theoretical wavefront. The difference was determined according to

$$\Phi_{error} = \Phi - \Phi_{wanted} . \tag{36}$$

The rms value of Φ_{error} was calculated using eq. (24). A limit for an approved surface of the mirror was defined as rms ≤ 0.8 rad. This rms value corresponds to a Strehl ratio of about 0.52 using eq. (29). The approved rms value should be obtained for either 12, 16, 20 or 25 modes.

Constant voltage bias

The transfer function was measured with a bias of 100, 141 or 152 V applied to all of the actuators simultaneously. This corresponds to a mirror surface bias with a large defocus and some astigmatism. The wavefronts attributed to the different bias and expressed in the first 10 Zernike coefficients are shown in Figure 18.

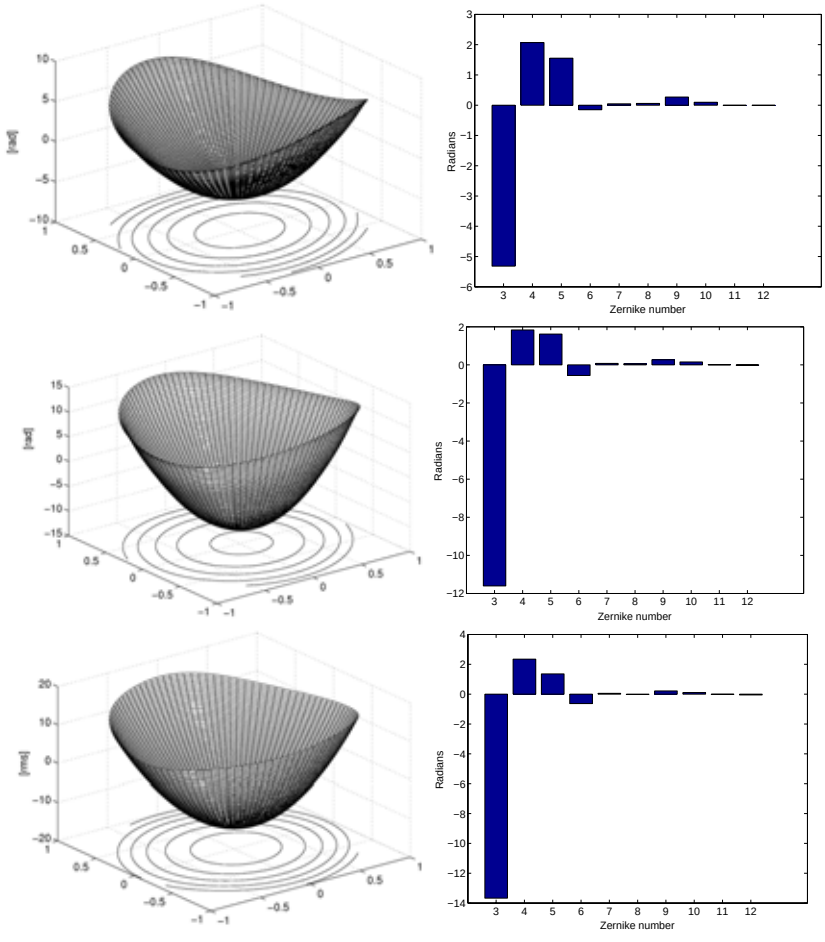

Figure 18 The surface corresponding to different voltage bias expressed in the first 10 Zernike coefficients The V_{bias} are from the top, 100, 141 and 152 V, respectively.

None of the transfer functions were able to produce an approved surface using open loop when no bias voltage was applied to the actuators. The surfaces that were generated was $\Phi_{wanted} = a_k \cdot z_k$ and a_k was varied between ±1 and ±7. The main part of the error was due to applying voltage to the actuators causing the mirror deforms in only one direction. This creates

a defocus, i.e. coefficient number three is less than zero and consequently affecting the the rms so that it becomes larger than 0.8.

When $\Phi_{wanted} = \Phi_{bias} + a_k z_k$ that is the deflection was measured compared to the bias and not a flat surface a better agreement between the constructed and wanted wavefront was obtained. Figure 19 shows the difference, in radians, between the largest and smallest coefficient that forms an approved surface ($rms \leq 0.8$) i.e. $a_{k,max}$-$a_{k,min}$. Three different intervals of the bias were compared. It is favourable to be in the middle range of the mirror working area which corresponds to a V_{bias} = 152 V. There is only one polynomial where the other transfer functions work better (defocus component). The largest advantage is achieved for polynomials number 9 and 10 (corresponding to the trefoil aberration).

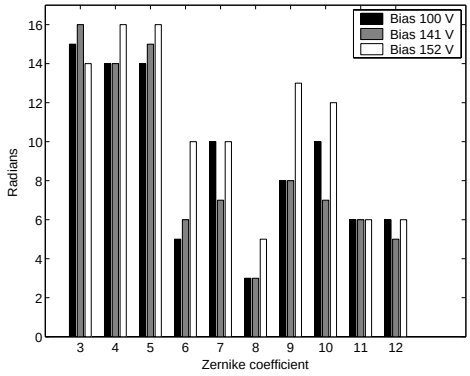

Figure 19 Difference between the largest and smallest coefficients with an approved area.

In Table 3 the maximum and minimum coefficient to produce approved surfaces for different Zernike polynomials i.e. $a_{k,min}$ and $a_{k,max}$ are shown. The minimum coefficient for the third Zernike polynomial is lowest for the bias with 100 V due to the fact that the deflection is measured relative to the bias. A coefficient of -9 rad for a bias of 100 V corresponds to -14 rad for the mirror whereas a coefficient of -5 rad for the bias of 152 V corresponds to -19 rad.

Table 3 Maximal and minimal coefficient values for different bias voltages and Zernike polynomials

Zernike no. (k)	**100 V**		**141 V**		**152 V**	
	$a_{k,min}$	$a_{k,max}$	$a_{k,min}$	$a_{k,max}$	$a_{k,min}$	$a_{k,max}$
3	-9	6	-6	10	-5	9
4	-6	8	-6	8	-8	8
5	-7	7	-8	7	-8	8
6	-1	4	-2	4	-5	5
7	-5	5	-4	3	-5	5
8	-1	2	-2	1	-3	2
9	-3	5	-3	5	-7	6
10	-5	5	-4	3	-6	6
11	-3	3	-3	3	-3	3
12	-3	3	-3	2	-3	3

Spherical bias

In order to investigate if the mirror works differently with a spherical bias a spherical surface was studied. The surface and its coefficients are shown in Figure 20. The theoretical bias was supposed to be $\Phi_{bias} = -14 z_3$ and was used when the coefficients were calculated. The measured bias had some contribution on other coefficients as indicated in Figure 20. The motivation to use -14 rad as a coefficient is that this number corresponds to the defocus coefficient for the bias with V_{bias} = 152 V.

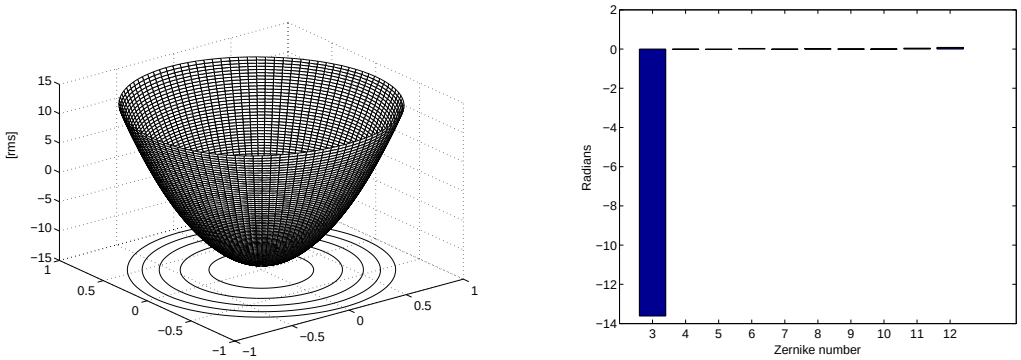

Figure 20 The surface of the spherical bias and the first 10 Zernike coefficients representing the surface.

Following the scheme for the bias with a constant voltage the deflection from the bias was measured. The limit for an approved surface was rms ≤ 0.8 rad. The distance between the largest and the smallest value of the coefficient that produce an approved surface is shown in Figure 21. In comparison, the coefficients with the bias of 141 and 152V are shown. The dynamics of the mirror using the spherical bias is less then when applying a bias with 152 V but larger in comparison to 141V bias.

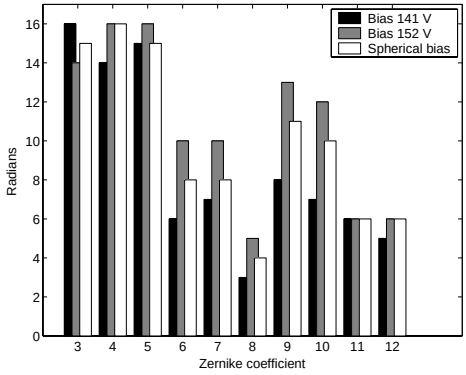

Zernike (no.)	$a_{k,min}$	$a_{k,max}$
3	-4	11
4	-6	10
5	-6	9
6	-4	4
7	-4	4
8	-2	2
9	-6	5
10	-5	5
11	-3	3
12	-3	3

Figure 21 Difference between largest and smallest coefficients with an approved area $a_{k,\max} - a_{k,\min}$ for the spherical bias (left). The maximum and minimum coefficient to produce approved surfaces, i.e. $a_{k,max}$ and $a_{k,min}$ for the spherical bias (right).

4.6 Closed loop

The closed loop scheme was used to investigate if the results from the Zernike production using the open loop scheme could be improved. The spherical bias was used since the defocus aberration introduced by the bias is easy to compensate for using e.g a passive optical component. All experiments were carried out with μ = 0.3, 0.5 and 1 and 12, 16, 20 and 25 of the mirror eigenmodes were used. The mirror shapes investigated were: i) defocus with $\phi_{wanted} = a_3 z_3$ and a_3 = 10, 11, 12, 13 and 14 rad, ii) astigmatism with $\phi_{wanted} = a_4 z_4$ and a_4 = 10, 11, 12 and 13 rad and iii) spherical aberration with $\phi_{wanted} = a_8 z_8$ and a_8 = 2, 3, 4, 5 and 6 rad. All iterations start by using the open loop to obtain an initial value.

4.6.1 Dependence of μ

In the closed loop scheme the gain factor μ determines how much the control signal changes per iteration. A larger μ gives a faster but less stable improvement. No significant problems with

fluctuations due to large μ values were observed. Figure 22 shows the rms value of the wavefront error using different values of μ. The rms error decreases rapidly for the first iterations and an equilibrium is reached. Table 4 shows how much the rms value improves in average for the different coefficients when 16 eigenmodes are used. The best choice is obtained with $\mu = 1$.

Table 4 Average enhancement of *rms* (Δrms) value with different μ[+]

	$\mu = 0.3$	$\mu = 0.5$	$\mu = 1.0$
Defocus	1.36	1.44	1.52
Astigmatism	0.48	0.49	0.60
Spherical aberration	0.30	0.31	0.34

[+)]All values are in rad and originates from experiments with 16 eigenmodes.

4.6.2 Number of eigenmodes

The number of eigenmodes used in the production of Zernike polynomials is important. This was clear even with the open loop scheme described above. In the closed loop scheme the number of eigenmodes had an even greater importance. With the surfaces producing defocus the results were as expected i.e. the rms value improved per iteration. The left plot in Figure 23 shows the rms value vs. iteration number when $\phi_{wanted} = 10z_3$. The number of modes makes a small difference but the results improve for all different number of modes. However, when producing a surface with astigmatism or a surface with spherical aberration the results depended highly on the number of modes. With 20 or 25 modes, the rms value could even increase from the initial value. The centre and the right plot in Figure 23 displays the rms value vs. iteration number for $\phi_{wanted} = 10z_4$ and $\phi_{wanted} = 2z_8$. For the astigmatic surface the rms value increases compared with the open loop value (the first iteration) when the number of eigenmodes are 20 or more.

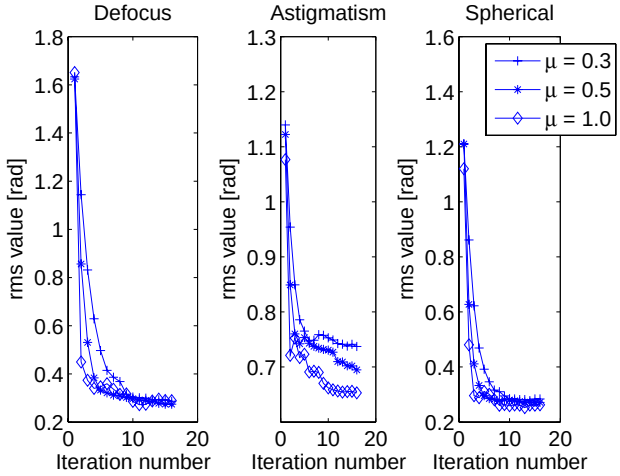

Figure 22 The rms improvements for different μ values. The rms is plotted versus the iteration number. Twelwe eigenmodes were used and the surfaces produced were (from left to right), $\phi_{wanted} = 10z_3$, $\phi_{wanted} = 10z_4$ and $\phi_{wanted} = 2z_8$.

For the spherical aberration the rms value increases after a few iterations when 20 eigenmodes are used. However, with 25 modes the rms values decreases and even reaches 0.2 where the iteration stops. With other Zernike coefficient values the results were quite similar. The defocus surfaces improved for all cases. There were no astigmatic surfaces whereas the rms value improved for 20 and 25 modes. In some of the experiments with astigmatism the rms value did not improve with respect to the initial value. For the surfaces with spherical aberrations the

number of modes that worked depended on the coefficient value. With $a_8 = 2$ using 12, 16 and 25 modes the results improved. With $a_8 = 3$ or 4 only 12 and 16 modes gives an improvement and when $a_8 = 5$ or 6 then the rms value increases after a few iterations even with 16 modes.

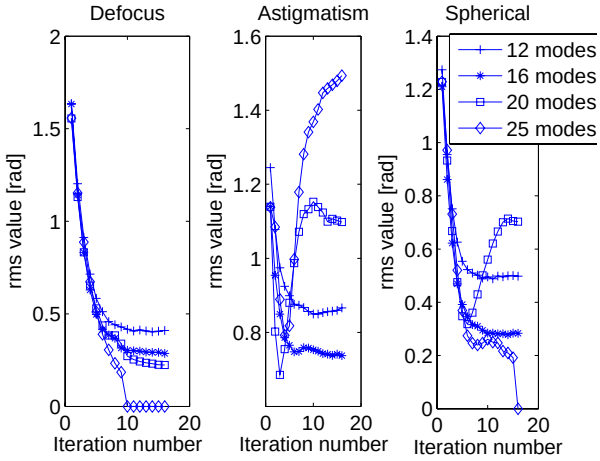

Figure 23 rms value for different number of eigenmodes using a closed loop scheme. The gain was $\mu = 0.3$ in all plots. The iteration was aborted when the rms value was less then 0.2 rad.

To further investigate why the closed loop might increase the rms values a measurement was performed with $\phi_{wanted} = 10z_4$ (astigmatism) and $\mu = 0.1$. A low μ was used to make sure that the divergence did not depend on a large μ value. The rms value increased for 20 and 25 modes as shown in the left plot in Figure 24. Hence the problem with increasing rms errors is not due to μ but most likely to the modes of high order. The results also show that after 30 to 40 iterations equilibrium is reached. If the rms value is divided into the component from the different Zernike polynomials it is clear that the largest part of the increasing rms value originates from the defocus component (Figure 24).

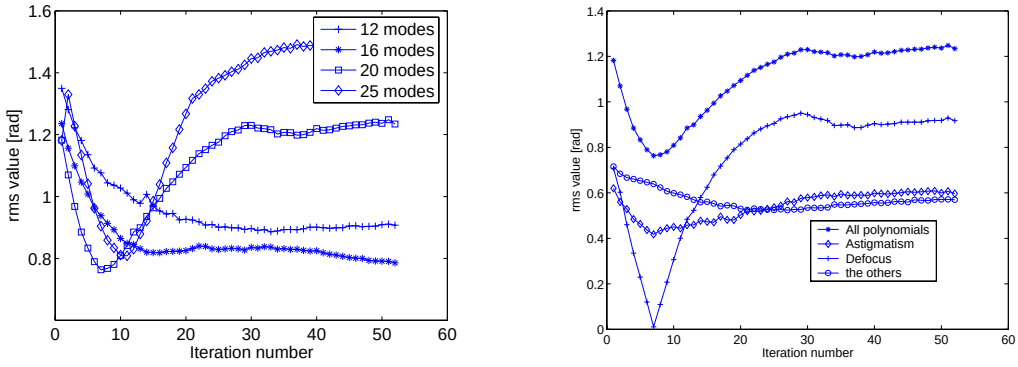

Figure 24 Investigations of closed loop rms values. The left plot shows the rms value for $\phi_{wanted} = 10z_4$ and $\mu = 1$. The right plot shows the rms value divided into the defocus and astigmatism components with 20 eigenmodes.

The conclusion that can be made from these results is that more than 20 modes causes instability to the system. Even 16 eigenmodes might cause instability and divergence. In the case where 16 modes cause instability the rms values are high even with 12 modes which indicate that the surface can not be produced by the mirror. Consequently, 16 modes give the best rms values in almost all the cases and can therefore be considered to be the best choice.

4.6.3 Improvement

All the Zernike polynomials that were produced were improved by using the closed loop (when 16 modes or less were used) approach. Table 5 shows the improvement of the rms value with 16

modes and μ = 1. In these cases the initial rms values were 1 < rms < 2. The largest improvement is caused by defocus (1.69 rad) but also the spherical aberration can improve if the coefficient is 2 or 3 rad. With the astigmatism the results improve less as shown in Table 5.

Table 5 Improvement of the rms value using closed loop. The results corresponds to μ = 1.0 and 16 eigenmodes. All values are in rad

a	Defocus	*a*	Astigmatism	*a*	Spherical
10	1.35	10	0.49	2	0.94
11	1.42	11	0.58	3	0.62
12	1.55	12	0.62	4	0.2
13	1.69	13	0.63	5	0.04
14	1.59	14	0.68	6	-0.11

5 DISCUSSIONS AND CONCLUSIONS

The spatial behaviour of a micromachined membrane deformable mirror has been investigated. Transfer functions corresponding to different voltage bias have been determined. The transfer functions were evaluated by testing the capability to produce wavefronts that can be described by different Zernike polynomials using an open loop scheme. In addition, a closed loop scheme has been investigated for three polynomials using spherical bias to study how much the mirror performance could be improved. It is important to remember that only one mirror was tested.

Wavefronts according to the first ten Zernike polynomials were produced by the mirror in order to obtain an understanding of how well the mirror could deform into different shapes. The Zernike polynomials were produced using an open loop scheme. Some of the polynomials were subsequently enhanced with a closed loop method. Several biases were investigated with the open loop scheme; constant voltage on all actuators (voltage 100, 141 and 152V) and a spherical bias Φ=-14z_3 rad. The bias with 152 V exhibited the best resolution i.e. the difference between the largest and the smallest Zernike coefficient that can be produced was largest. The spherical bias had a good resolution too and is probably the best choice since it only leaves a spherical aberration which can be corrected by a lens. The PV value of the spherical bias was slightly less then the PV value for the bias with 152 V. This fact probably explains why the spherical bias does not give as good results as the 152 V bias.

The low order Zernike polynomials, defocus and astigmatism, could be produced with large coefficients values. It seems like the polynomials having a radial part of the power of three (polynomials 6, 7, 9 and 10) the bias with 152 V is more important to use then for the other polynomials. The closed loop scheme can enhance the open loop results. The magnitude of the enhancement depends on the conditions. In the case of defocus to create ϕ_{wanted} = 10z_3 with the bias ϕ_{wanted} = -14z_3 means that the mirror surface is ϕ = -4z_3. This surface should be quite easy to achieve but starting with the bias it becomes more difficult. In this case, the closing of loop creates a big difference. In the cases of astigmatism and spherical aberration the enhancement is not as large. With the open loop the results varied with respect to the optimal number of eigenmodes. However, with the closed loop it became obvious that when using 20 modes or more the system was not stable. This need to be further investigated but with the results available it seems as if 16 modes is the best choice.

If the same voltage was applied to the mirror several consecutive times the results were identical. However, if the same voltage was applied to the mirror with a few days difference the results varied somewhat (typically the rms value changed with about 0.1 rad over a week). This

is probably due to small changes in the interferometer. The main error sources which need to be considered include; aberrations in the interferometer, the aperture applied by the software (i.e. the region of the interferogram that was analyzed) might not be perfectly centred and the fact that the superposition principle for the different actuators is an approximation.

Aberrations in the interferometer are probably the largest error source. The aberrations depend both on errors when aligning the interferometer and on imperfections in the components. The error in alignment is probably the main reason for why the values change over time. The errors due to the misplacement of the software aperture are not very large. A short experiment was done where the aperture was moved with 10 pixels in both the x and y direction. The difference in the Zernike coefficient values were less then or equal to 0.23 rad and the average difference was 0.10 rad. When the aperture was moved 10 additional pixels the difference was doubled. Finally, the fact that the superposition principle is not completely accurate is the reason why the closed loop scheme should improve the results. If the mirror was perfectly linear and the superposition assumption was totally accurate there would not be a need for the closed loop.

In conclusion, a deformable membrane mirror was tested. Four different transfer functions were used, where the one with V_{bias}= 152V had the highest resolution. Zernike polynomials were produced with coefficient values reaching from 2 to 11 rad depending on the polynomial. A closed loop scheme was tested and improved the results significantly. The number of the mirrors eigenmodes that were used in the transfer function had a great influence on the result.

6 APPENDIX 1

6.1 The least square method

The least square method is a scheme to determine the best solution to an over-determined equation system. We want to solve the system

$$\mathbf{A}\bar{\mathbf{x}} = \bar{\mathbf{b}} \tag{37}$$

where A is a mxn matrix and b is a column vector with m elements. Since the equation is over determined, m > n, the error becomes

$$\bar{\mathbf{r}} = \bar{\mathbf{b}} - \mathbf{A}\bar{\mathbf{x}} \,. \tag{38}$$

The aim of the method is to minimize the square of this error

$$\left\|\bar{\mathbf{r}}\right\| = \sum_{i=1}^{m} r_i^2 \,. \tag{39}$$

The solution is obtained by solving the equation

$$\mathbf{A}^T\mathbf{A}\bar{\mathbf{x}} = \mathbf{A}^T\bar{\mathbf{b}} \,. \tag{40}$$

This equation has a unique solution. For a proof of this statement the reader is referred to a standard text book in numerical analysis, e.g. ref[18].

6.2 Zernike polynomials

There are several different ways to number the polynomials. The reason for using the order presented in this appendix is that Quick Fringe uses it.

Table 6 Zernike polynomials

Term	n	m	Function polar coordinates
0			1
1	1	1	$\rho \cos\theta$
2			$\rho \sin\theta$
3		0	$2\rho^2 - 1$
4	2	2	$\rho^2 \cos(2\theta)$
5			$\rho^2 \sin(2\theta)$
6		1	$(3\rho^2 - 2)\rho \cos\theta$
7			$(3\rho^2 - 2)\rho \sin\theta$
8		0	$6\rho^4 - 6\rho^2 + 1$
9	3	3	$\rho^3 \cos(3\theta)$
10			$\rho^3 \sin(3\theta)$
11		2	$(4\rho^2 - 3)\rho^2 \cos(2\theta)$
12			$(4\rho^2 - 3)\rho^2 \sin(2\theta)$
13		1	$10\rho^4 - 12\cos\rho^2 + 3$
14			$10\rho^4 - 12\cos\rho^2 + 3$
15		0	$20\rho^6 - 12\rho^4 + 12\rho^2 - 1$
16	4	4	$\rho^4 \cos(4\theta)$
17			$\rho^4 \sin(4\theta)$
18		3	$(5\rho^2 - 4)\rho^3 \cos(3\theta)$
19			$(5\rho^2 - 4)\rho^3 \sin(3\theta)$
20		2	$(15\rho^2 - 4)\,\rho^3 \cos(3\theta)$
21			$(15\rho^2 - 4)\,\rho^3 \sin(3\theta)$
22		1	$(35\,\rho^6 - 60\,\rho^4 + 30\rho^2 - 4)\rho \cos\theta$
23			$(35\,\rho^6 - 60\,\rho^4 + 30\rho^2 - 4)\rho \sin\theta$
24		0	$70\rho^8 - 140\rho^6 + 90\rho^4 - 20\rho^2 + 1$
25	5	5	$\rho^5 \cos(5\theta)$
26			$\rho^5 \sin(5\theta)$
27		4	$(6\rho^2 - 5)\rho^4 \cos(4\theta)$
28			$(6\rho^2 - 5)\rho^4 \sin(4\theta)$
29		3	$(21\rho^7 - 30\rho^5 + 10\rho^3)\cos(3\theta))$
30			$(21\rho^7 - 30\rho^5 + 10\rho^3)\sin(3\theta))$
31		2	$(56\rho^8 - 105\rho^6 + 60\rho^4 - 10\rho^2)\cos(2\theta)$
32			$(56\rho^8 - 105\rho^6 + 60\rho^4 - 10\rho^2)\sin(2\theta)$
33		1	$(126\rho^9 - 280\rho^7 + 210\rho^5 - 60\rho^3 + 5\rho)\cos(\theta)$
34			$(126\rho^9 - 280\rho^7 + 210\rho^5 - 60\rho^3 + 5\rho)\sin(\theta)$
35		0	$252\rho^{10} - 630\rho^8 + 560\rho^6 - 210\rho^4 + 30\rho^2 - 1$
36	6	0	$924\rho^{12} - 2772\rho^{10} + 3150\rho^8 - 1680\rho^6 + 420\rho^4 - 42\rho^2 + 1$

6.3 Program source code

6.3.1 Matlab code transforming an interferogram into Zernike coefficients

```
function [x] = image2zernike(impath)

%Get the interferogram images from file
inter = imread(impath);

% Cut out the interferogram from the image
inter = inter(140:960,230:1050);

% Set the number of lines from the added tilt in the interferogram whith a
% flat mirror
number_of_lines = 54;

% Reduce the window to the inner 64%
s = size(inter,1); inter = inter(0.18*s:0.82*s, 0.18*s:0.82*s);
```

```
% Normalize the interferogram
inter = (double(inter));
inter = (inter-(min(min(inter))));
inter = (inter/max(max(inter))-0.5);

% Shrink the image to 400*400 pixels
s = size(inter,2);
inter = interp2(inter,1:(s/400):s,(1:(s/400):s)');
s = size(inter,2);

% Add a circular aperture
for i = 1:s
   for j = 1:s
      if (sqrt((i-s/2)^2 + (j-s/2)^2)) > (s/2)
         inter(i,j) = 0;
      end
   end
end

% Fourier transform
Inter = fft2(inter);

% Move the quadrants, to have origo in the middle.
Inter2 = fftshift(Inter);
f = number_of_lines - 1;

% Translate the fourier transform, and filter it.
skal = 1.2;
Inter3 = [zeros(s,f) Inter2(:,1:(s-f))];
Inter4 = [zeros(s,(s/2-f/skal))  Inter3(:,(s/2-f/skal):(s/2+f/skal)) zeros(s,(s/2-f/skal))];

Inter5 = fftshift(Inter4);

% Use the invers fourier transform, and pick out the angel.
phase = angle(ifft2(Inter5));

% Add a circular aperture
for i = 1:s
   for j = 1:s
      if (sqrt((i-s/2)^2 + (j-s/2)^2)) > (s/2)
         phase(i,j) = -pi;
      end
   end
end

% Unwrap the phase in the x-direction
phase = unwrap(phase,[],2);

% Unwrap the phase in the y-direction
phase(200:400,:) = unwrap(phase(200:400,:)); phase2 =
imflip(phase(1:200,:)); phase2 = unwrap(phase2); phase =
[imflip(phase2) ; phase(201:400,:)];

% Reduce the size of the field to decrease the calculation time
s = size(phase,2);
phase = interp2(phase,1:(s/200):s,(1:(s/200):s)');

% Add a circular appertur
s = size(phase,2) maxi = phase(100,100);
for i = 1:s
   for j = 1:s
      if (sqrt((i-s/2)^2 + (j-s/2)^2)) > (s/2);
         phase(i,j) = maxi;
      end
   end
end
```

```
% Reduce the phase to 100*100, and transform it into polar coordinates
phase = interp2(phase,1:2:200,(1:2:200)');

x = [-1:2/99:1];
y = [-1:2/99:1];
[X,Y] = meshgrid(x,y);
[Theta,R,Phase] = cart2pol(X,Y,phase);

% Make a matrix of zernike polynomials

z(1:100,1:100)     = R.*cos(Theta);  %x
z(1:100,101:200)   = R.*sin(Theta);  %y
z(1:100,201:300)   = 2*R.^2-1;
z(1:100,301:400)   = R.^2.*cos(2*Theta);
z(1:100,401:500)   = R.^2.*sin(2*Theta);
z(1:100,501:600)   = (3*R.^3-2*R).*cos(Theta);
z(1:100,601:700)   = (3*R.^3-2*R).*sin(Theta);
z(1:100,701:800)   = 6*R.^4-6*R.^2+1;
z(1:100,801:900)   = R.^3.*cos(3*Theta);
z(1:100,901:1000)  = R.^3.*sin(3*Theta);
z(1:100,1001:1100) = (4*R.^4-3*R.^2).*cos(2*Theta);
z(1:100,1101:1200) = (4*R.^4-3*R.^2).*sin(2*Theta);
z(1:100,1201:1300) = (10*R.^5-12*R.^3+3*R).*cos(Theta);
z(1:100,1301:1400) = (10*R.^5-12*R.^3+3*R).*sin(Theta);
z(1:100,1401:1500) = 20*R.^6-30*R.^4+12*R.^2-1;
z(1:100,1501:1600) = R.^4.*cos(4*Theta);
z(1:100,1601:1700) = R.^4.*sin(4*Theta);
z(1:100,1701:1800) = (5*R.^5-4*R.^3).*cos(3*Theta);
z(1:100,1801:1900) = (5*R.^5-4*R.^3).*sin(3*Theta);
z(1:100,1901:2000) = (15*R.^6-20*R.^4+6*R.^2).*cos(2*Theta);
z(1:100,2001:2100) = (15*R.^6-20*R.^4+6*R.^2).*sin(2*Theta);
z(1:100,2101:2200) = (35*R.^7-60*R.^5+30*R.^3-4*R).*cos(Theta);
z(1:100,2201:2300) = (35*R.^7-60*R.^5+30*R.^3-4*R).*sin(Theta);
z(1:100,2301:2400) = 70*R.^8-140*R.^6+90*R.^4-20*R.^2+1;
z(1:100,2401:2500) = R.^5.*cos(Theta*5);
z(1:100,2501:2600) = R.^5.*sin(Theta*5);
z(1:100,2601:2700) = (6*R.^6-5*R.^4).*cos(4*Theta);
z(1:100,2701:2800) = (6*R.^6-5*R.^4).*sin(4.*Theta);
z(1:100,2801:2900) = (21*R.^7-30.*R.^5+10*R.^3).*cos(3*Theta);
z(1:100,2901:3000) = (21*R.^7-30.*R.^5+10*R.^3).*sin(3*Theta);
z(1:100,3001:3100) = (56*R.^8-105*R.^6+60*R.^4-10*R.^2).*cos(2*Theta);
z(1:100,3101:3200) = (56*R.^8-105*R.^6+60*R.^4 -10*R.^2).*sin(2.*Theta);
z(1:100,3201:3300) = (126*R.^9-280*R.^7+210*R.^5-60*R.^3+5*R).*cos(Theta);
z(1:100,3301:3400) = (126*R.^9-280*R.^7+210*R.^5-60*R.^3+5*R).*sin(Theta);
z(1:100,3401:3500) = 252*R.^10-630*R.^8+560*R.^6-210*R.^4+30*R.^2-1;
z(1:100,3501:3600) = 924*R.^12-2772*R.^10+3150*R.^8-1680*R.^6+420*R.^4-42*R.^2+1;
z(1:100,3601:3700) = 1;

% Add a circular aperture to all of the polynomials
for i = 1:100
   for j = 1:100
      if R(i,j) > 1
         z(i,j:100:3700) = 0;
         Phase(i,j) = 0;
      end
   end
end

% Use least square method to fit the phase to zernike polynomial
for i = 0:99
   A((i*100+1):((i+1)*100),1:37) = z(1:1:100,(i+1):100:3700);
end for i = 0:99
   b(i*100+1:(i+1)*100,1) = Phase(1:1:100,i+1);
end

x = -lsqr(A,b,1e-9,100);
```

6.3.2 Control program for the mirror

```
#include <windows.h>
#include <stdio.h>
#include <stdlib.h>
#include <winioctl.h>
#include <iostream.h>
#include "ClassDriver.h"
#include <stddef.h>
#include <conio.h>

#define BASE_ADDRESS_2 0xDC00
#define BASE_ADDRESS_1 0xD800

_declspec(dllexport) float voltout(long volt_in[]);
_declspec(dllexport) float voltout(long volt_in[])

{
   int i;
   int error;
   int konv[38];
   konv[1] = 13;
   konv[2] = 21;
   konv[3] = 10;
   konv[4] = 14;
   konv[5] = 2;
   konv[6] = 1;
   konv[7] = 9;
   konv[8] = 20;
   konv[9] = 22;
   konv[10] = 11;
   konv[11] = 12;
   konv[12] = 7;
   konv[13] = 4;
   konv[14] = 5;
   konv[15] = 3;
   konv[16] = 0;
   konv[17] = 15;
   konv[18] = 8;
   konv[19] = 23;

   konv[20] = 9;
   konv[21] = 23;
   konv[22] = 22;
   konv[23] = 21;
   konv[24] = 8;
   konv[25] = 4;
   konv[26] = 2;
   konv[27] = 7;
   konv[28] = 5;
   konv[29] = 3;
   konv[30] = 1;
   konv[31] = 0;
   konv[32] = 15;
   konv[33] = 14;
   konv[34] = 13;
   konv[35] = 12;
   konv[36] = 11;
   konv[37] = 10;


// Create Handle
   CDriver PortDriver("\\\\.\\PORTIO1");
    PortDriver.Open(1, BASE_ADDRESS_1, 0x0080);
```

```
    PortDriver.Open(2, BASE_ADDRESS_2, 0x0080);

   for (i = 0; i<19; i++)
   {
      if(PortDriver.Write(1, BASE_ADDRESS_1+(konv[i+1]*4), volt_in[i])!=0)
         error = 1;
      // i = 0 => kanal 1 = 0+1
   }
   for (i = 19; i<37; i++)
   {
      if(PortDriver.Write(2, BASE_ADDRESS_2+(konv[i+1]*4), volt_in[i])!=0)
         error = 1;
      //i = 19 => kanal 1 = 19-18

   }
   if (error ==1)
         return (1);
   else
      return (0);
}
\end{verbatim}
\end{scriptsize}
```

7 REFERENCES

[1] Tyson, R. (1991) Principle of adaptive optics, Academic Press, Inc., USA.

[2] McGraw-Hill electronical edition, Adaptive optics.

[3] Eriksson, E. (2004Low-order aberration correction with a membrane deformable mirror for adaptive optics Göteborg. Sweden.

[4] www.okotech.com

[5] Goodman, J. (1996) Introduction to fourier optics, Singapore. McGraw-Hill.

[6] Tyson, R. (2000) Adaptive optics engineering handbook, USA. Marcel, Dekker, Inc.

[7] Takeda, M. Ina, H. \& Kobayashi, S. (1981). Fourier-transform method of fringe-pattern analysis for computer-based topography and interferometry. Optical Society of America. 72(1), 156-160

[8] Quick Fringe, Fringe analysis softwareVersion 4.x

[9] Wyant, J. Creath, K. (1992) Basic Wavefront Aberration Theory for Optical Metrology, University of Arizona, Tucson, Arizona

[10] Zhu,L. et.al. (1999). Adaptive control of a micromachined continuous-membrane deformable mirror for aberration compensation. Applied optics 38 (1), 168-176

[11] Fernández, E. Artal, P. (2003). Optics express11 (9), 1056-1069

[12] Råde, L \& Westergren, B. (1998). Mathematics Handbook for Science and Engineering. 4th ed. Lund. Sweden. Studentlitteratur.

[13] A short course in adaptive optics}. (21-23 May 2003) Course material. The photonics group. Imperial College. London.

[14] Mahajan, V. (1983). Strehl ratio for primary aberrations in te*rms* of their aberration variance. Optical Society of America 73 (9), 860-861.

[15] Zho, L. et.al.(1999). Wave-frontgeneration of Zernike polynomial modes with amicromachined membrane deformable mirror. Appliedoptics 38 (28), 6019-6026

[16] Vdovin, G Sarro, P.M. (1995). Flexible mirror micromachined in silicon. Applied optics, 34 (16), 2968-2972

[17] Paterson, C., Munro, I. Dainty, J. C. (2000). A low cost adaptive optics system using a membrane mirror. Optical express 9 (6), 175-185.

[18] Eldén, L. Wittmeyer-Koch, L. (1996). Numerisk analys - en introduktion (3rd ed.). Lund. Studentlitteratur.